The Effect of Preload and Surface Roughness Quality on Linear Joint Model Parameters

Hassan Jalali, Hamed Haddad Khodaparast, Michael I Friswell

College of Engineering, Swansea University, Bay Campus, Fabian Way, Crymlyn Burrows, Swansea, SA1 8EN, United Kingdom

Abstract

The physical parameters of the contact interfaces, such as preload and surface roughness quality, significantly affect the stiffness of joints. Knowledge of the relationship between these interface parameters and the equivalent stiffness allows joints to be considered in the design stages of complex structures. Hence, this paper considers the effect of contact interface parameters on the identified equivalent stiffness parameters of joint models. First, a new generic joint model is proposed to model the contact interfaces. Then, the ability of three different joint models, including the new model proposed in this paper, to capture the linear effects of contact interfaces under different preloads and surface roughness qualities is investigated. Finally, it is concluded that the preload and surface roughness quality control the normal and shearing stiffness of the joint models respectively. Experimental investigations also reveal that a complex mechanism governs the energy dissipation in the contact interface.

Keywords: structural joint, surface roughness, preload

1. Introduction

The dynamic response of assembled structures is governed by the physics of their contact interfaces in the joints. Analysing the behaviour of the assembled structures is difficult because of the complexities in the inherent physics and due to many parameters affecting the dynamics of the contact interface. Joints play an important role in the overall damping and stiffness of assembled structures in structural dynamics. They are used to transfer forces and moments between different components through their frictional contact interfaces. Despite huge research efforts during the past decades [1] [2], the dynamic behaviour of friction

is not yet fully understood. This is mainly because there are several parameters with a high level of uncertainty [3] that affect the dynamic behaviour of friction, including the contact interface preload, the finish quality of the contact surfaces, temperature and humidity variation, sensitivity to the order of tightening several joints in a structure, etc. Variation in these parameters affects the linear, as well as the nonlinear, behaviour of the contact interfaces [4].

Investigations into both the effective linear representation and the nonlinear behaviour of contact interfaces have been studied by many researchers. Several methods have been proposed to consider contact interfaces in assembled structures. Joints can be modelled using simple lumped elements, such as springs [5], or zero-thickness elements [6] [7] [8]. These zero-thickness joint elements include the effect of the contact interface at each point and define the linear/nonlinear constitutive relation between two adjacent points in the FE/analytical model of the structure. Alternatively, the joints can be modelled by using thin-layer [9] or generic joint elements [10] [11] [12] [13]. These types of joint models consider the effect of the contact interface over a finite length of the structure. Bograd *et al.* gave a comprehensive literature survey on different methods of modelling joints [14].

The problem of the contact between rough surfaces has been studied by many researchers in the past [15] [16] [17] [18] [19]. The relationship between the normal and tangential contact stiffnesses of nominally flat surfaces with respect to normal contact pressure has been investigated theoretically, numerically and experimentally [20] [21] [22]. Goerke and Willner [23] used simulated and experimental case studies to address the effects of surface roughness and geometrical irregularities on the stiffness of joints in the normal direction.

In this paper the equivalent linear stiffness modelling of contact interfaces is investigated. The contribution of this paper is twofold. First, a parametric rectangular generic joint model is proposed to model bolted lap joints by using the decomposition of the stiffness matrix of an initial element. Second, the effects of bolt preload and contact surface roughness quality on the dynamic characteristics of assembled structures is investigated by using simulated and experimental case studies. The ability of different joint models, including the model presented in this paper, to model contact interfaces under different bolt preloads and different contact surface roughness qualities is examined.

2. Contact Interface Mechanisms

Several mechanisms may be activated at the contact interface of a joint in the normal and tangential directions [24], as shown schematically in Figure 1. Activation of contact interface mechanisms depends mainly upon the amplitude of the external forces applied. Generally, at low level excitation forces, the joint behaviour is linear and linear models can be used. Nonlinear effects arise when high amplitude excitation forces are applied: the different nonlinear mechanisms involved at the contact interface and their interactions mean that appropriate models must be developed.

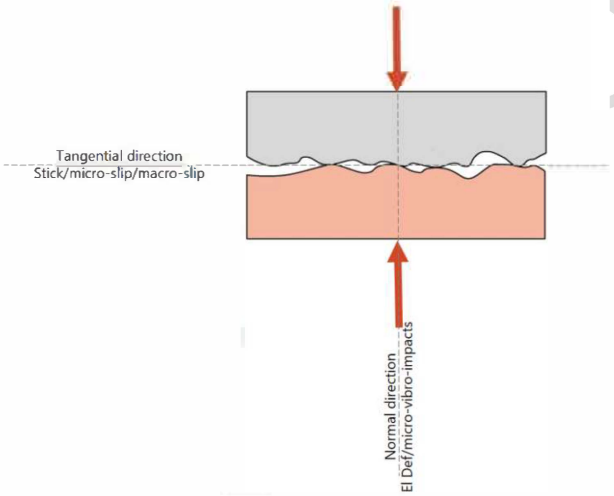

Figure 1. Different mechanisms that occur at a contact interface

In the normal direction, a contact interface generally gives an elastic deformation, i.e. a linear behaviour, at low excitation force amplitudes. When the amplitude of the excitation forces increases, micro-vibro-impacts can occur at the contact interface which results in the transfer of energy to higher frequencies, which is a nonlinear behaviour [25] [26]. In contrast, in the tangential direction, the contact interface can be in stick (linear), micro-slip (nonlinear) or macro-slip (nonlinear) conditions at low, medium and high excitation force amplitudes, respectively [27] [28]. Linear models of joints target linear contact interface stiffness in the normal and tangential (shearing) directions.

It is worth mentioning that in bolted lap-joints the bolt preload creates pre-stress in the contacting substructures. One way to deal with this pre-stress is to consider geometric stiffness effects. The alternative way, which is used in this paper, is to incorporate the effects of pre-stress into an interfacial element and the proposed element in this paper is actually aimed at modelling this pre-stress. In other words,

the normal and tangential stiffness of the contact interface is the result of applying preload (or pre-stress) which is considered by the formulation of the proposed joint element in the following sections. Also, the linear behaviour of the contact interface will be considered in this paper which assumes that the nonlinear mechanisms don't activate in the contact interface. Interfacial separation [29] usually happens when nonlinear mechanisms and especially micro-vibro-impacts are active in the contact interface. The activation of the nonlinear slip and micro-vibro-impact mechanisms is the result of applying high amplitude forcing to the structure [30]. In this paper it is assumed that the excitation force amplitudes are low enough to prevent activation of nonlinear mechanisms in the contact interface. Therefore in this paper the effects of interfacial kinematics are ignored.

3. Linear Joint Modelling Methods

Two methods are often used to develop an equivalent model of the joint section in an assembled structure, as shown in Figure 2. In this figure, an assembled structure (Figure 2a) and its FE models are shown. In the FE models the contact interface is modelled with 4-noded rectangular joint elements (Figure 2b) and/or 2-noded beam-like joint elements (Figure 2c). The former modelling approach is known as the thin layer element modelling method in the literature [9], where a layer of 2D/3D solid elements is used to model the contact interface. A suitable constitutive equation must be defined for the joint elements. A general constitutive equation for a 3D solid element with orthotropic material is given by

$$\begin{Bmatrix}\sigma_{xx}\\ \sigma_{yy}\\ \sigma_{zz}\\ \sigma_{xy}\\ \sigma_{yz}\\ \sigma_{zx}\end{Bmatrix} = \begin{bmatrix} E_{11} & E_{12} & E_{13} & & & \\ & E_{22} & E_{23} & & & \\ & & E_{33} & & & \\ & & & E_{44} & & \\ & & & & E_{55} & \\ & & & & & E_{66}\end{bmatrix} \begin{Bmatrix}\epsilon_{xx}\\ \epsilon_{yy}\\ \epsilon_{zz}\\ \epsilon_{xy}\\ \epsilon_{yz}\\ \epsilon_{zx}\end{Bmatrix} \quad (1)$$

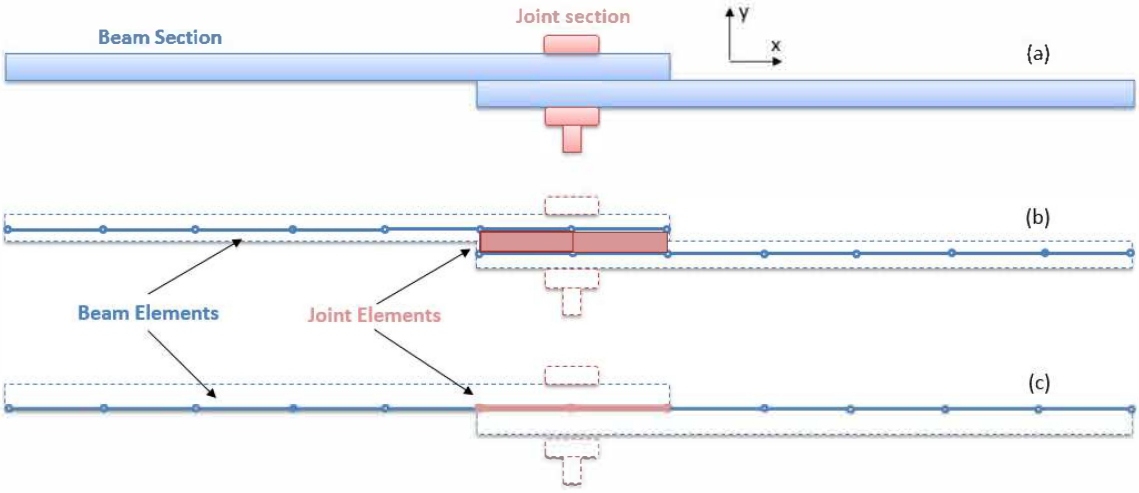

Figure 2. Modelling the joint in an assembled structure (a): 4-noded rectangular joint elements (b) and 2-noded beam-like joint elements (c)

Thin layer elements have been used to model the linear [31] [32] [12] and nonlinear [33] [34] [35] effects of joints by many researchers. In a series of papers, Ahmadian *et al.* [31] [32] [12] employed the thin layer element theory to model the linear behaviour of contact interfaces in structures. They considered isotropic material for the joint elements, which reduces the unknown parameters in the constitutive equation to two and these parameters were identified using model updating techniques. The two parameters are the elastic modulus, E, and the shear modulus, G, of the joint elements which control the normal and tangential stiffness of the contact interface, respectively.

Mayer and Gaul [9] and Bograd *et al.* [14] applied constraints on the constitutive equation based on a physical understanding of the contact interfaces. They set the off-diagonal terms equal to zero, since there is no transverse contraction produced by the contact interface. Also, the stiffness of the contact interface parallel to the joint's surface is negligible, which means that $E_{11} = E_{22} = 0$. The in-plane shearing of the contact interface is also negligible, i.e. $E_{66} = 0$. Thus, there remain two independent parameters that define the contact interface: the normal stiffness, E_{33}, and the tangential stiffness, $E_{44} = E_{55}$, which control the behaviour of the contact interface in normal and tangential directions respectively.

The second approach to joint modelling uses 2-noded beam-like elements to model the joint section. Ahmadian and Jalali [36] obtained the structural mass, damping and stiffness matrices of a 2-noded beam-like element, called a generic joint element, by ensuring that the necessary conditions for matrices of a

structural element were satisfied. The stiffness matrix of this element has two unknown parameters to capture the effects of the normal and tangential behaviour of the contact interface.

In the next section, a new joint modelling method based on the decomposition of the stiffness matrix is proposed which can be used to construct the formulation of the joint modelling approaches described in this section.

4. Proposed Joint Modelling Method

The method introduced in this paper is based on the decomposition of the stiffness matrix representing the joint. Decomposition methods often use a different basis for decomposition and two are briefly reviewed here. In the standard decomposition method, any stiffness matrix $[K_0]$ is decomposed into its static eigenvalues and eigenvectors given by [37] [38]

$$[K_0]_{n\times n} = [U_0]_{n\times n}[\Lambda_0]_{n\times n}[U_0]^T_{n\times n} \tag{2}$$

where $[U_0]_{n\times n}$ is the matrix of unit normalized static eigenvectors, i.e. $[U_0]^T[U_0] = [I]$, and $[\Lambda_0]_{n\times n}$ is a diagonal matrix containing static eigenvalues. Since the stiffness matrix is semi-positive definite, some of the eigenvalues are zero. There are also non-standard decomposition methods which have been proposed in certain circumstances for solving specific problems. For example, Doebling *et al.* [39] proposed a method that decomposed the stiffness matrix in a non-standard form as,

$$[K_0]_{n\times n} = [A]_{n\times m}[Z]_{m\times m}[A]^T_{m\times n} \tag{3}$$

where, in contrast to Equation (2), $[A]_{n\times m}$ and $[Z]_{m\times m}$ are not given by the eigenvalues and eigenvectors but are obtained by using a specific algorithm. In their method, decomposition of a global stiffness matrix is carried out using standard decomposition in an elemental stage. Generally, $[Z]$ contains different elemental stiffness parameters, and columns of $[A]$ represent the connectivity of the structure by defining how a particular element stiffness parameter influences the stiffness at structural DOF. The interested reader is referred to [39] for more details.

Gladwell and Ahmadian [40] formulated a family of generic elements by adopting the decomposition method given by Equation (2). An alternative

parametric stiffness matrix can be formulated for an element by substituting the dynamic eigenvectors of the element, rather than the static eigenvectors, to give

$$[K]_{n\times n} = \left([M_0]_{n\times n}[U]_{n\times n}\right)[\Lambda]_{n\times n}\left([M_0]_{n\times n}[U]_{n\times n}\right)^T \tag{4}$$

where $[\Lambda] = \mathrm{diag}([\lambda_1, \lambda_2, ..., \lambda_n])$ is the matrix of eigenvalues and [U] contains the free-free mass-normalized vibration modes of the element, obtained from

$$([K_0] - \lambda[M_0])\{u\} = 0 \tag{5}$$

where $[M_0]$ is the mass matrix of the original element, and only the non-zero eigenvalues are used, i.e. $\lambda \neq 0$.

Since there is no mass effect imposed by the contact interface, static and dynamic eigenvalues/eigenvectors of the elements representing the joint contact interface are the same. Therefore, a new parametric stiffness matrix to model joints in structural dynamics can be formulated as

$$[K_J]_{n\times n} = [U_0]_{n\times n}[\bar{\Lambda}]_{n\times n}[U_0]^T_{n\times n} \tag{6}$$

Here, the eigenvectors correspond to the non-zero eigenvalues of the stiffness matrix of the original element are combined with a matrix of parametric eigenvalues $[\bar{\Lambda}]_{n\times n}$ to construct a parametric stiffness matrix for a joint element. It is worth mentioning that by substituting the eigenvalues of the original stiffness matrix in equation (6), i.e. $[\bar{\Lambda}] = [\Lambda_0]$, the original stiffness matrix $[K_J] = [K_0]$ is recovered. Basically, the parametric eigenvalues in equation (6) can be used to adjust FE models of structures containing contact interfaces. It is also possible to relate the eigenvalues to different physical parameters at the contact interfaces. This will be done in this paper using experimental results.

To clarify the differences between the decomposition methods described in above, the stiffness matrix of a dynamical system is decomposed. Consider a 2 DOF mass-spring system of Figure 3 with mass and stiffness matrices as

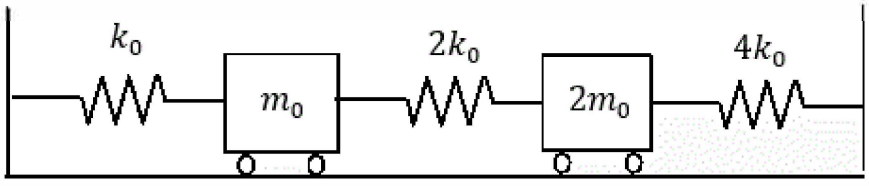

Figure 3- 2DOF mass-spring system

$$[M_0] = m_0\begin{bmatrix}1 & 0\\ 0 & 2\end{bmatrix}, [K_0] = k_0\begin{bmatrix}3 & -2\\ -2 & 6\end{bmatrix} \tag{7}$$

Based on the standard decomposition method, the eigenvalues and eigenvectors of the stiffness matrix, i.e. Equation (2), the stiffness matrix can be decomposed as

$$[U_0][\Lambda_0][U_0]^T = \frac{1}{\sqrt{5}}\begin{bmatrix}2 & -1\\ 1 & 2\end{bmatrix}\begin{bmatrix}2k_0 & 0\\ 0 & 7k_0\end{bmatrix}\frac{1}{\sqrt{5}}\begin{bmatrix}2 & 1\\ -1 & 2\end{bmatrix} \tag{8}$$

If the method proposed by Doebling *et al*. [39] is used, one obtains

$$[K_0] = \frac{1}{\sqrt{2}}\begin{bmatrix}1 & 1 & 0\\ 0 & -1 & -1\end{bmatrix}\begin{bmatrix}2k_0 & 0 & 0\\ 0 & 4k_0 & 0\\ 0 & 0 & 8k_0\end{bmatrix}\frac{1}{\sqrt{2}}\begin{bmatrix}1 & 0\\ 1 & -1\\ 0 & -1\end{bmatrix} \tag{9}$$

Stiffness matrix decomposition using the dynamic eigenvectors and eigenvalues proposed by Gladwell and Ahmadian [40] results in

$$([M_0][U])[\Lambda]([M_0][U])^T = \sqrt{m_0}\begin{bmatrix}-\frac{1}{\sqrt{2}} & \frac{1}{\sqrt{2}}\\ 1 & 1\end{bmatrix}\left(\frac{k_0}{m_0}\begin{bmatrix}3+\sqrt{2} & 0\\ 0 & 3-\sqrt{2}\end{bmatrix}\right)\sqrt{m_0}\begin{bmatrix}-\frac{1}{\sqrt{2}} & 1\\ \frac{1}{\sqrt{2}} & 1\end{bmatrix} \tag{10}$$

Similarly, parametric stiffness matrices for this 2 DOf mass-spring system can be considered using different decomposition methods as

$$[K]_s = \begin{bmatrix}4s_1 + s_2 & -2(s_2 - s_1)\\ -2(s_2 - s_1) & s_1 + 4s_2\end{bmatrix} \tag{11}$$

$$[K]_d = \begin{bmatrix}d_1 + d_2 & -\sqrt{2}(d_1 - d_2)\\ -\sqrt{2}(d_1 - d_2) & 2(d_1 + d_2)\end{bmatrix} \tag{12}$$

$$[K]_z = \begin{bmatrix}z_1 + z_2 & -z_2\\ -z_2 & z_2 + z_3\end{bmatrix} \tag{13}$$

where $[K]_s$, $[K]_d$ and $[K]_z$ are parametric stiffness matrices obtained using static eigenvectors, dynamic eigenvectors [40] and the method proposed by Doebling *et al*. [39]. s_i, d_i and z_i $(i = 1,2)$ are stiffness parameters used for constructing stiffness matrices in equations (11-13). It is worth mentioning that the two first

parametric stiffness matrices are useful in model updating and the last one in damage detection.

5. Generic Joint Elements

In this section, the method based on decomposition of the stiffness matrix proposed in the previous section is demonstrated to obtain the stiffness matrices of 2-noded and 4-noded generic joint elements.

5.1. Beam-like generic joint element

To introduce the beam-like generic joint element, first the 2-noded Euler-Bernoulli beam element shown in Figure 4 is considered. The beam element has mass per unit length ρA, flexural rigidity EI and length L. The element mass and stiffness matrices are

$$[K_0]_{4\times 4} = \frac{EI}{L^3}\int_0^1 [B(\zeta)][B(\zeta)]^T \mathrm{d}\zeta \tag{14}$$

$$[M_0]_{4\times 4} = \rho AL\int_0^1 [N(\zeta)][N(\zeta)]^T \mathrm{d}\zeta \tag{15}$$

where $\zeta = x/L$ and x is the position on the beam. The strain-displacement matrix $[B(\zeta)]$ is defined as $[B(\zeta)] = \mathrm{d}^2[N]/\mathrm{d}\zeta^2$ and the matrix of shape functions $[N(\zeta)]$ is

$$[N(\zeta)] = [\chi]\{b(\zeta)\} \tag{16}$$

where

$$[\chi] = \begin{bmatrix} 2 & -3 & 0 & 1 \\ L & -2L & L & 0 \\ -2 & 3 & 0 & 0 \\ L & -L & 0 & 0 \end{bmatrix}, \quad \{b(\zeta)\} = [\zeta^3 \quad \zeta^2 \quad \zeta \quad 1]^T \tag{17-18}$$

The eigenvectors of the stiffness matrix may be partitioned into the rigid-body and strain modes of the element. The element stiffness matrix of the beam has rank 2, and hence the element has two rigid-body or zero strain modes. The rigid body modes are denoted by $\psi_1(\zeta)$ and $\psi_2(\zeta)$, and $\psi_3(\zeta)$ and $\psi_4(\zeta)$ are two orthogonal strain modes and defined as,

$$\{\psi(\zeta)\} = \begin{Bmatrix}\{\psi(\zeta)\}_r \\ \{\psi(\zeta)\}_s\end{Bmatrix} = [\psi_1(\zeta) \quad \psi_2(\zeta) \quad \psi_3(\zeta) \quad \psi_4(\zeta)]^T = [S]\{b(\zeta)\} \quad (19)$$

where

$$[S] = \begin{bmatrix} 0 & 0 & 0 & 1 \\ 0 & 0 & L & -L \\ 2(L+4/L) & -3(L+4/L) & L & 2/L \\ 0 & L & -L & 0 \end{bmatrix} \quad (20)$$

The rigid body and strain modes of the element are shown in Figure 4. Note that the strain modes are orthogonal over the length of the element, and hence $\int_0^1 \psi_3(\zeta)\,\psi_4(\zeta)\mathrm{d}\zeta = 0$. The strain modes are used to construct the stiffness matrix of a beam-like generic element, from Equation (6) as

$$[K_G]_b = f_1(p_1,p_2,...,p_m)\{u_3\}\{u_3\}^T + f_2(p_1,p_2,...,p_m)\{u_4\}\{u_4\}^T \quad (21)$$

In general, f_1 and f_2 are positive valued functions governing the behaviour of the 2-noded element. $p_i,\ i = 1,2,...,m$ can be attributed to geometrical and material properties of the element. $\{u_3\}$ and $\{u_4\}$ are defined as

$$[\bar{u}] = \begin{bmatrix}\{u_3\}^T \\ \{u_4\}^T\end{bmatrix} = \begin{bmatrix}\{\psi(0)\}_s & \{\psi(0)'\}_s & \{\psi(1)\}_s & \{\psi(1)'\}_s\end{bmatrix} \quad (22)$$

where $\{\psi(\zeta)'\}_s = \frac{1}{L}\mathrm{d}\{\psi(\zeta)\}_s/\mathrm{d}\zeta$. $[\bar{u}]$ is then obtained as,

$$[\bar{u}] = \begin{bmatrix} 2/L & 1 & -2/L & 1 \\ 0 & -1 & 0 & 1 \end{bmatrix} \quad (23)$$

The mode orthogonality means that $\{u_3\}^T\{u_4\} = 0$. The stiffness matrix of a Euler-Bernoulli beam element can be constructed using Equation (21) by taking $f_1 = 3EI/L$ and $f_2 = EI/L$.

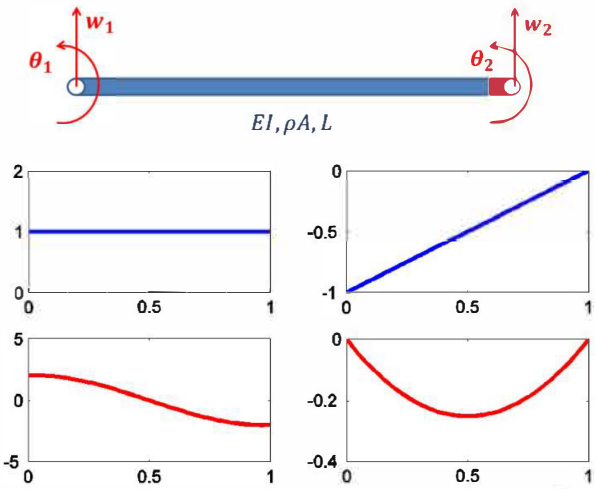

Figure 4. The 2-noded beam element and its rigid-body (in blue) and strain (in red) modes

The stiffness matrix defined in Equation (21) can be used to model the joint section in structures like the one described in Figure 2. The two parameters f_1 and f_2 in the stiffness matrix control the normal and tangential stiffness of the contact interfaces respectively. It is worth mentioning that parameters f_1 and f_2 represent the effects of the contact interface stiffness and it is not possible to relate them directly to the actual physical contact interface stiffness in the normal and tangential directions. By substituting $f_1 = k_w L^2/4$ and $f_2 = k_\theta L^2$ into Equation (21), the stiffness matrix of the generic joint element proposed by Ahmadian and Jalali [36] is obtained. They regarded f_1 and f_2 as independent parameters representing the lateral and torsional stiffness of the element respectively, that define the normal and shear stiffness of the contact interface.

5.2. 4-noded rectangular generic joint element

This approach is identical to that for the beam-like generic joint element described in the previous section. First the stiffness matrix of the 2D plane element shown in Figure 5 is obtained. The element is a rectangular element with a, b and t being its length, width and thickness respectively. The stiffness matrix is obtained as,

$$[K_0]_{8\times 8} = abt\int_0^1\int_0^1 [B(\zeta_1,\zeta_2)]^T[E][B(\zeta_1,\zeta_2)]\mathrm{d}\zeta_1\mathrm{d}\zeta_2 \qquad (24)$$

where $\zeta_1 = x/a$, $\zeta_2 = y/b$ and $[B(\zeta_1,\zeta_2)]$ is the strain-displacement matrix of the element which is obtained from its shape functions [41]. The element shape functions are defined as,

$$[N_1 \quad N_2 \quad N_3 \quad N_4]^T = [\chi]\{b(\zeta_1,\zeta_2)\} \tag{25}$$

where,

$$[\chi] = \begin{bmatrix} 1 & -1 & -1 & 1 \\ -1 & 1 & 0 & 0 \\ 1 & 0 & 0 & 0 \\ -1 & 0 & 1 & 0 \end{bmatrix}, \quad \{b(\zeta_1,\zeta_2)\} = [\zeta_1\zeta_2 \quad \zeta_1 \quad \zeta_2 \quad 1]^T \tag{26-27}$$

$[B(\zeta_1,\zeta_2)]$ is obtained as,

$$[B(\zeta_1,\zeta_2)] = [\boldsymbol{\Gamma}N_1 \quad \boldsymbol{\Gamma}N_2 \quad \boldsymbol{\Gamma}N_3 \quad \boldsymbol{\Gamma}N_4], \quad \boldsymbol{\Gamma} = \begin{bmatrix} \frac{1}{a}\partial/\partial\zeta_1 & 0 \\ 0 & \frac{1}{b}\partial/\partial\zeta_2 \\ \frac{1}{b}\partial/\partial\zeta_2 & \frac{1}{a}\partial/\partial\zeta_1 \end{bmatrix} \tag{28}$$

$[E]$ in Equation (24) is the stress-strain relationship matrix, which was given in Equation (1) for the general case of a 3D orthotropic material. $[E]$ can be obtained for plane-stress or plane-strain cases in 2D problems. In the present paper, plane-strain is assumed as this more accurately represents the joint model used. *t* is the element thickness.

In the following, a 4-noded rectangular generic joint element is proposed for contact interfaces by using the stiffness matrix of Equation (24). To introduce the generic element formulation of the stiffness matrix, the strain modes of the 4-noded element are needed which are obtained by decomposing the stiffness matrix of Equation (24). In general, the modes of a rectangular element may be functions of element dimensions and/or material properties, as is the stiffness matrix defined in Equation (24). However, in the case of a square element, i.e. $a = b$, the modes are no longer functions of material properties. Since the stiffness matrix of a 4-noded generic joint element should not be a function of material properties, a combination of different modes of a rectangular element which are not functions of material properties and modes of a square element are used in the following and formulation of generic joint element is obtained. Figure 5 shows different modes including the rigid-body modes, i.e. $[U_r]$, and the strain

modes, i.e. $[U_0]$, of a 4-noded square plane (or joint) element. The strain modes are divided into shear-stress $[U_{0d}]$ modes (in red) and normal-stress $[U_{0n}]$ modes (in blue). The same classification applies to the case of a rectangular element.

For a rectangular element, the rigid-body modes $[U_r]$ are only functions of the element dimensions, as Equation (29) shows. The strain modes can be divided into two modes, namely $[U_{0d}]$ and $[U_{0n}]$. Like $[U_r]$, the columns of $[U_{0d}]$ are only functions of element dimensions, whereas the columns of $[U_{0n}]$ are functions of both element dimensions and material properties, i.e. $[E]$. However, when the element is square, i.e. $a = b$, the columns of $[U_{0n}]$ are no longer functions of material properties as was described in the previous paragraph. Therefore, the matrix of modes of the element, which will be used later to construct a generic joint element, is given by

$$[[U_r]_{8\times 3} \quad [U_{0d}]_{8\times 3} \quad [U_{0n}]_{8\times 2}] = \begin{bmatrix} b/a & 1 & -b/a & a/b & 0 & -1 & -1 & 1 \\ 0 & 0 & 1 & 1 & -1 & 0 & -1 & -1 \\ b/a & 1 & -b/a & a/b & 0 & 1 & 1 & -1 \\ 1 & 0 & 0 & -1 & 1 & 0 & -1 & -1 \\ 0 & 1 & 0 & -a/b & 0 & -1 & 1 & -1 \\ 1 & 0 & 0 & -1 & -1 & 0 & 1 & 1 \\ 0 & 1 & 0 & -a/b & 0 & 1 & -1 & 1 \\ 0 & 0 & 1 & 1 & 1 & 0 & 1 & 1 \end{bmatrix} \tag{29}$$

In fact, the first six modes in equation (29) are modes of a rectangular element, and the last two modes are from a square element. The modes presented in equation (29) are depicted for a square element in Figure 5.

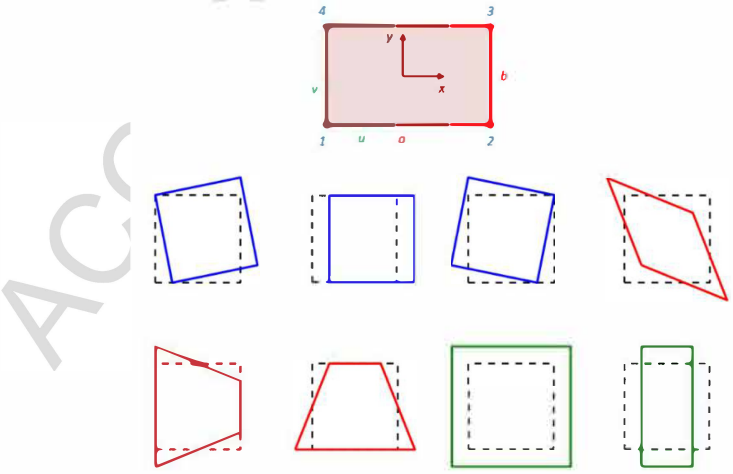

Figure 5. The 4-noded plane element and its corresponding modes: rigid-body $[U_r]$ (in blue), shear stress strain $[U_{0d}]$ (in red) and normal stress strain $[U_{0n}]$ (in green) for the case of $a = b$

It is worth mentioning that the strain modes presented in Equation (29) are orthogonal, i.e. $\{U_{0,i}\}^T\{U_{0,j}\} = 0,\ i \neq j$. Therefore, mathematically they can be used as a base for constructing the stiffness matrix of a joint element. This means that any deformation of a joint element in real situations can be considered as a linear combination of its deformation in free-free cases which are defined in strain modes of Equation (29). The method proposed in Equation (6) suggests that a parametric stiffness matrix with parameters assigned to each strain mode may be constructed. Applying this method to the element presented in Figure 5 results in a stiffness matrix having 5 different parameters which cannot be physically justifiable. Also, several parameters of the element introduce difficulties in the identification stage.

Therefore, to obtain a stiffness matrix for a 4-noded generic joint element with minimum but efficient parameters, the strain modes of Equation (29) are categorized into two sets based on their physical meaning and then one parameter is attributed to each set which is easily justifiable. As it was explained in the previous sections, two main mechanisms can be active at the contact interface of joints in normal and tangential (or shear) directions. This means that physically two parameters are enough to control the state of the contact interface model. On the other hand, Figure 4 shows that $[U_{0n}]$contains the modes where the element experiences normal stress and $[U_{0d}]$contains the modes where the element undergoes shear stress. Based on the nature of the strain modes explained above and the behaviour of the contact interfaces described in the previous sections, one may consider the formulation of a new rectangular generic joint element as

$$[K_G]_p = [\overline{U}_{0n}][\overline{U}_{0n}]^T k_n + [\overline{U}_{0d}][\overline{U}_{0d}]^T k_d \tag{30}$$

where columns of $[\overline{U}_{0n}]$ and $[\overline{U}_{0d}]$ are normalized mode shapes having being obtained by using the modes presented in Equation (29) such that $[\overline{U}_{0n}]^T[\overline{U}_{0n}] = [I]$ and $[\overline{U}_{0d}]^T[\overline{U}_{0d}] = [\Lambda]$ where,

$$[\Lambda] = \begin{bmatrix} (b/a)^2 + 1 & 0 & 0 \\ 0 & 1 & 0 \\ 0 & 0 & 1 \end{bmatrix} \tag{31}$$

The stiffness matrix proposed in equation (30) is symmetrical and semi-positive definite and, as will be verified in the next sections, can effectively capture the linear behaviour of the contact interfaces in shear and normal directions.

The parameters k_n and k_d in Equation (30) control the normal and shear stiffness of the contact interface, respectively.

The strategy employed for constructing stiffness matrix can also be used for the damping matrix of the 4-noded rectangular generic joint element shown in Figure 5. It is well known that the slip mechanism in tangential direction mainly contributes to the energy dissipation in the contact interface. Therefore, in this paper, it is proposed to use the shear stress strain modes, i.e. $[U_{0d}]$, to construct a damping matrix for the joint element as,

$$[C_G]_p = [\overline{U}_{0d}][\overline{U}_{0d}]^T c_d \tag{32}$$

where c_d controls the energy dissipation in the contact interface and can be identified by using experimental/numerical results.

The new joint element formulation proposed in this section is used in the following sections to model contact interfaces in numerical and experimental case studies.

6. Numerical case study

In this section the applicability of the proposed generic elements in modelling the contact interface in a jointed structure is examined. The aim of this paper is to investigate the effect of surface roughness quality on joint model parameters. To this end, a simple example is used to demonstrate this effect. Therefore, in this section, the intention is to investigate how different joint models can trace the changes made in the contact interface.

A steel ($E = 210$ GPa, $\upsilon = 0.31$ and $\rho = 7800$ kg/m^3) assembled structure composed of two beam sections connected through a contact interface is modelled in *Ansys* (Figure 6). The beam sections are 3mm thick and 30mm wide, but their lengths are different, one is 200mm and the other is 250mm. The beams have 30mm of overlapped interface contact.

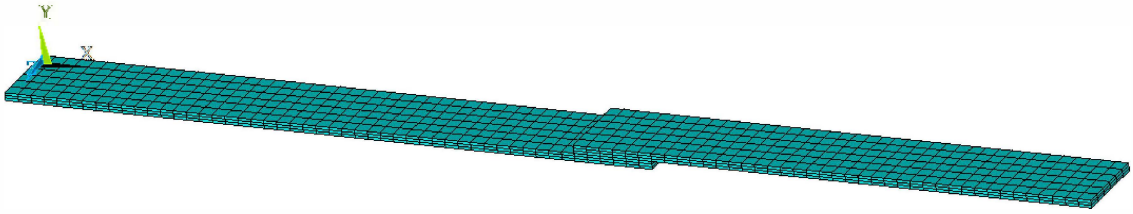

Figure 6. Schematic of the FE model

Solid186 elements are used to model the beam sections of the structure. The contact condition between the two beam sections is considered node-to-node contact and is modelled by employing COMBIN14 elements which represent the contact as a combination of linear spring elements in x, y and z directions as k_x, k_y and k_z. It is assumed that a uniform preload is applied to the contact interface.

The aim of using this example is to investigate the ability of the joint models introduced in previous section to capture the effect of the preload in the contact interface. The linear contact behaviour in the interface of the simulated example shown in Figure 6 is modelled using linear springs in x, y and z directions which represent normal stiffness, i.e. $k_y = K_N/n_e$, and tangential stiffness, i.e. $k_x = k_z = K_T/n_e$, of the contact interface. $n_e = 49$ is the number of spring elements in each direction at the contact interface. The effect of the preload will be considered in the spring stiffness values as described in the following paragraph.

Based on the results presented in [22], for moderate and high nominal closure pressures p, i.e. $p \geq 50$ MPa, a linear relationship between normalized normal and tangential contact stiffnesses vs. closure pressure can be considered, i.e. k_N and $k_T \propto p$. Nominal closure pressure and normalized normal/tangential contact stiffness are obtained as $p = \frac{P}{A}\left(\frac{\mathrm{N}}{\mathrm{m}^2}\right)$, $k_N = \frac{K_N}{A}\left(\frac{\mathrm{N}}{\mathrm{m}^3}\right)$ and $k_T = \frac{K_T}{A}\left(\frac{\mathrm{N}}{\mathrm{m}^3}\right)$ where P is the preload of the contact interface, A is the contact surface area and K_N and K_T are normal and tangential contact stiffnesses. Medina et al. [42] showed that in the case of exponential distribution of asperity peak heights with standard deviation , the normalized tangential stiffness varies linearly with contact pressure as,

$$k_T = \frac{4(1-\upsilon)\ p}{\sqrt{\pi}(2-\upsilon)\sigma} \tag{33}$$

It should be noted that the tangential stiffness is independent of Young's modulus of the contacting bodies. As previous studies show [22], tangential-to-normal contact stiffness is only a function of Poisson's ratio υ. The tangential-to-normal

contact stiffness for the contact surfaces made from the same materials can be considered as [22]

$$\frac{K_T}{K_N} = \chi \frac{1-\upsilon}{2-\upsilon} \tag{34}$$

where $0.5 \leq \chi \leq 2$. Greenwood and Williamson [16], Krolikowski and Szczepek [18] and Mindlin [15] obtained $\chi = 2$, Sherif and Korsa [20] proposed $\chi = \pi/2$ and Yoshioka and Scholz [43] reached a value of 0.71 for χ.

Following the above discussion and considering $\chi = \pi/2$ based on Sherif and Korsa [20], $\upsilon = 0.31$ for contact bodies made of steel and $\sigma = 4.6$ μm, the stiffness of each spring element in normal and tangential directions of the contact interface in FE model shown in Figure 6 are considered as,

$$k_x = k_z = 2 \times 10^5 P \left(\frac{\mathrm{N}}{\mathrm{m}}\right), \quad k_y = 7.7 \times 10^5 P \left(\frac{\mathrm{N}}{\mathrm{m}}\right) \tag{35}$$

Equation (34) shows that the state of contact interface is considered a function of preload only and by changing the preload, dynamic characteristics of the assembled structure change too. The change in the normalized bending natural frequencies, i.e. ω/ω_{ref}, in the X-Y plane (i.e. Figure 6) by changing the contact interface preload P is shown in Figure 7. Natural frequencies are normalized by using the natural frequencies corresponding to $P = 0.5\mathrm{N}$ which are referred to as ω_{ref} in Figure 7 and are tabulated in Table 1.

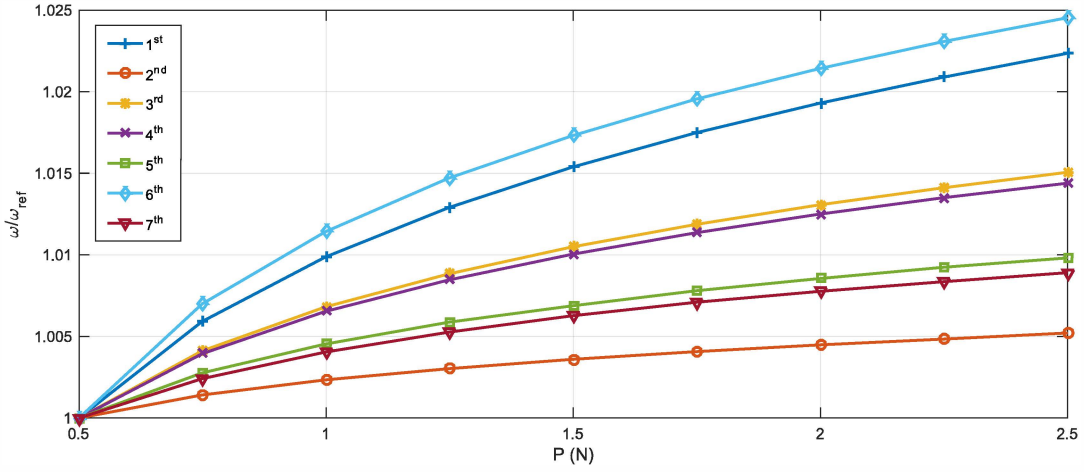

Figure 7. Changes in bending natural frequencies in the X-Y plane by changing preload P

Table 1- Reference natural frequencies ω_{ref} corresponding to $P = 0.5$N, (Hz)

1st	2nd	3rd	4th	5th	6th	7th
88.98	247.82	478.10	793.79	1191.30	1650.80	2200.70

Figure 7 shows that by changing the preload P the rates of change in natural frequencies are different. The 2nd natural frequency has the lowest rate of change (0.5%) and the 6th natural frequency has the highest (2.5%). The natural frequencies presented in Figure 7 are used later in this paper to obtain the parameters of the joint models introduced in the previous sections.

6.1. FE modelling and stiffness parameter identification

FE models of the structure shown in Figure 6 are constructed by using the Euler-Bernoulli beam elements introduced in Equations (14) and (15) and the joint elements defined by equations (24) and (30). Beam and joint elements are used respectively for modelling beam sections and joint part of the structure as depicted in Figure 2. A reasonably fine mesh is used by taking the element's length equal to *2.5*mm to keep the discretisation error at a minimum level.

The joint section is considered in the FE model using three different types of joint models: the beam-like generic joint model introduced in Equation (21) (*model#1*), the rectangular generic joint model introduced in Equation (30) (*model#2*) and the model proposed by Bograd et al. [14] (*model#3*). The stiffness matrix of the joint model proposed by Bograd et al. [14] is obtained by using Equation (24) when $[E]$ is considered as,

$$[E] = diag([E_{xx} \quad E_{yy} \quad G_{xy}]),\ E_{xx} \ll 1 \tag{36}$$

The natural frequencies of FE models, i.e. $\{\omega_a\}$. are obtained by free vibration analysis using Equation (37)

$$[\overline{M}]\{\ddot{d}\} + ([\overline{K}] + [\overline{K}]_J)\{d\} = \{0\} \tag{37}$$

where $[\overline{M}]$, $[\overline{K}]$ and $[\overline{K}]_J$ are the global mass and stiffness matrices of the beams and joint sections of the structure respectively.

The unknown parameters of the joint models (i.e. the joint parameters) are identified by minimizing the differences between the simulated natural frequencies presented in Figure 7, i.e. $\{\omega_e\}$, and the natural frequencies obtained from FE models containing joint models *model#1*, *model#2* and *model#3*, i.e. $\{\omega_a\}$. Parameter identification is carried out by employing the first order eigenvalue sensitivity method which uses the following equation in an iterative scheme to find the joint parameters [44]

$$[S]\{\theta\} = \{\epsilon\} \tag{38}$$

where $[S]$ is the matrix of sensitivity of different natural frequencies to the joint parameters, $\{\theta\}$ is the vector of corrections to the joint parameters in each iteration and $\{\epsilon\}$ is the vector of differences between experimental and numerical natural frequencies. For example, for an FE model containing joint model *model#2* the sensitivity matrix is,

$$[S] = \begin{bmatrix} \left(\varphi_1^T \frac{\partial[\overline{K}]_J}{\partial k_n}\varphi_1\right)/\omega_{e1}^2, & \left(\varphi_1^T \frac{\partial[\overline{K}]_J}{\partial k_d}\varphi_1\right)/\omega_{e1}^2 \\ \vdots & \vdots \\ \left(\varphi_r^T \frac{\partial[\overline{K}]_J}{\partial k_n}\varphi_r\right)/\omega_{er}^2, & \left(\varphi_r^T \frac{\partial[\overline{K}]_J}{\partial k_n}\varphi_r\right)/\omega_{er}^2 \end{bmatrix}, \{\theta\} = \begin{Bmatrix} \delta k_n \\ \delta k_d \end{Bmatrix}, \{\epsilon\} = \begin{Bmatrix} (\omega_{e1}^2 - \omega_{a1}^2)/\omega_{e1}^2 \\ \vdots \\ (\omega_{er}^2 - \omega_{ar}^2)/\omega_{er}^2 \end{Bmatrix} \tag{39}$$

where r is the number of natural frequencies used in identification and φ_r is the mode shapes obtained using Equation (37). Equation (38) is solved for $\{\theta\}$ by minimizing the norm of the error vector $\{\epsilon\}$ which results in

$$\{\theta\} = ([S]^T[S])^{-1}[S]^T\{\epsilon\} \tag{40}$$

The identified joint parameters for different joint models are presented in Figure 8. It is worth mentioning that since the state of the contact interface in a numerical example is controlled by only one parameter, i.e. the preload P, logically one parameter is sufficient in each joint model to capture the effect of preload. This is true for *model#2* and *model#3* as the results presented in Figure 8 show. In fact, identification of the second parameters in *model#2* and *model#3* results in a very low value compared to the first parameter which means that the second parameter is not effective. Therefore, for these models only one parameter being both from

the same nature- i.e. both parameters control the normal stiffness in contact interface- is shown in Figure 8. Joint models *model#2* and *model#3* represent only the contact interface but the joint model *model#1* represents both beams and the contact interface in the joint section (Figure 2). That is why both parameters in joint model *model#1*, i.e. f_1 and f_2, have non-zero values as Figure 8 shows.

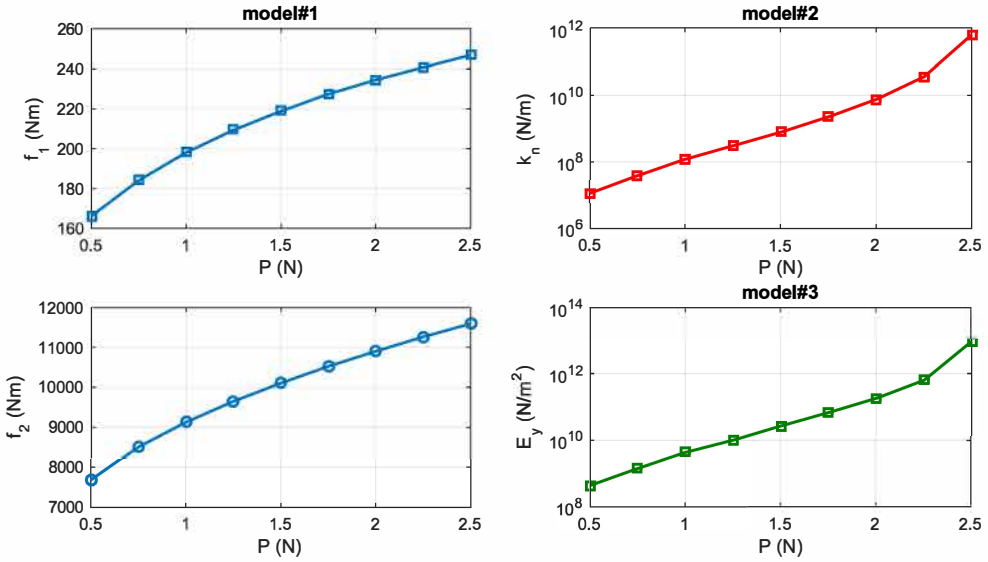

Figure 8. Identified joint model parameters

The norm of the vector of differences between two sets of natural frequencies, i.e. $|e| = |(\{\omega_a\} - \{\omega_e\})/\{\omega_e\}|$, is shown in Figure 9 for the different joint models.

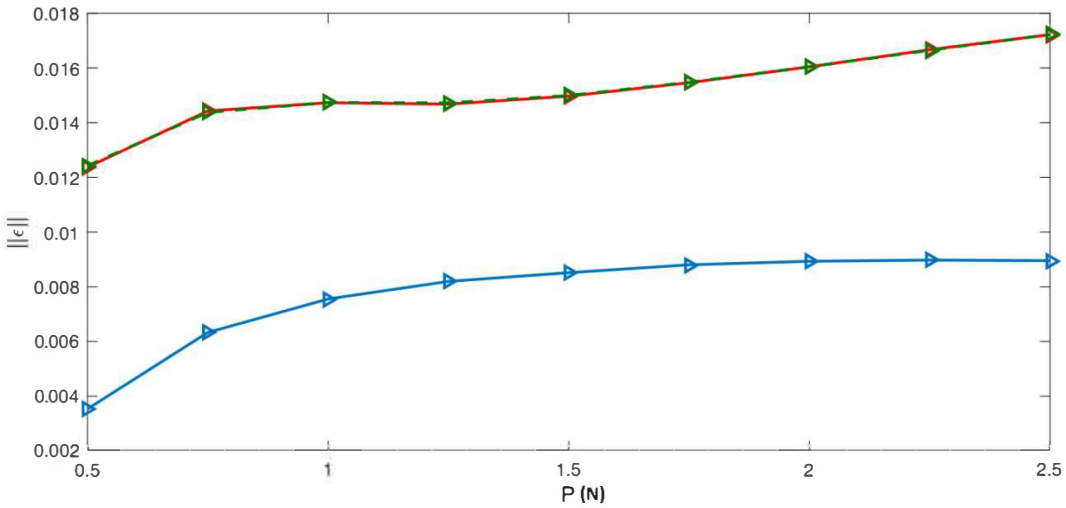

Figure 9. Norm of error vector $|e|$: *model#1* (blue), *model#2* (red) and *model#3* (green)

Figure 9 shows that although all joint models predict the characteristics of the contact interface with a reasonable accuracy, joint model *model#1* is the most accurate model and the accuracies of *model#2* and *model#3* are at a same level.

6.2. Damping parameter identification

To examine the capability of the proposed damping model of Equation (32) in representing the energy dissipation at the contact interface, the FE model shown in Figure 6 is used. As stated in the previous sections, the slip mechanism is responsible for almost all the energy dissipation in the contact interface of joints. To incorporate this energy dissipation in the FE model, viscous damping elements are considered in parallel to the spring elements in tangential directions, i.e. c_x and c_z, of the contact interface in the FE model. By using the damped FE model, direct FRFs, i.e. $h^e(\omega)$, at the end of the beam are obtained by considering two different values for viscous damping coefficients as shown in Figure 10. The results presented in Figure 10 correspond to the case when k_x, k_y and k_z are obtained for $P = 2.25\text{N}$ and $c_x = c_z = 100\text{Ns/m}$ (Figure 10a) and $c_x = c_z = 750$ Ns/m (Figure 10b).

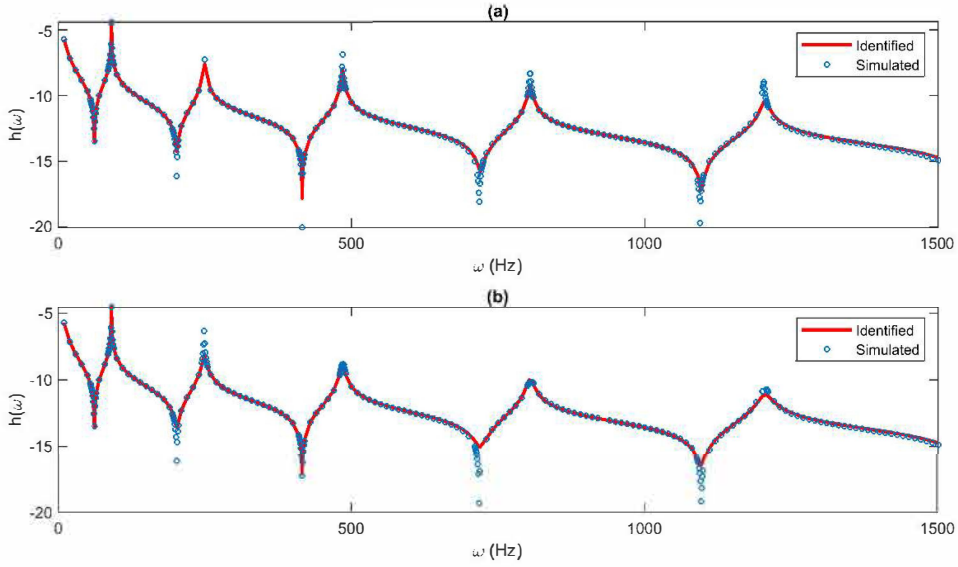

Figure 10. Comparison of the simulated and identified FRFs: $c_d = 110\text{Ns/m}$ (a) and $c_d = 225\text{Ns/m}$ (b).

Having obtained the simulated FRFs, the identification of the joint model damping coefficient is now considered. A simplified dynamic model of the damped structure shown in Figure 6 can be constructed by employing the Euler-Bernoulli beam elements introduced in Equations (14) and (15) and the stiffness and damping matrices of the 4-noded rectangular generic joint element defined by equations (30) and (32) as,

$$[\overline{M}]\{\ddot{d}\} + [\overline{C}]_J\{\dot{d}\} + ([\overline{K}] + [\overline{K}]_J)\{d\} = \{f(t)\} \tag{41}$$

In equation (41) $[\overline{K}]_J$ is considered known based on the results presented in the previous section. By using equation (41), the matrix of Frequency Response Functions (FRFs) is obtained as,

$$[H(\omega)] = \left([\overline{K}] + [\overline{K}]_J + j\omega[\overline{C}]_J - \omega^2[\overline{M}]\right)^{-1} \tag{42}$$

Equation (42) is used to obtain the direct FRFs at the end of the beam structure, i.e. $h^a(\omega)$. Finally, the unknown parameter of the joint damping matrix, i.e. c_d, is identified by minimizing the norm of the differences between simulated and analytical FRFs, i.e. $E_h = \|h^e(\omega) - h^a(\omega)\|$. Damping parameter identification is done in this paper using a direct search method. The identified FRFs are compared with the simulated FRFs in Figure 10. The results presented in this figure indicate that the proposed damping model can represent the energy dissipation in the contact interface. In the next section an experimental case study is considered.

7. Experimental case study

To check the capability of the joint models introduced in previous sections to model contact interfaces in real structures, experimental case studies are considered in this section. In the experimental case studies, 4 assembled beam-like structures with similar material and geometric properties are prepared. The beams are made from cold rolled stainless steel and their dimensions are shown in Figure 11.

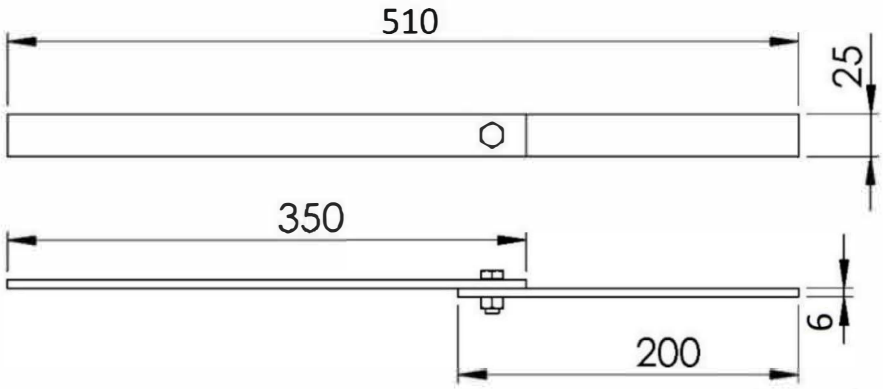

Figure 11. Dimensions of the experimental test structures, mm

To investigate the effects of joint contact surface quality on the identified joint model parameters, four assembled structures with identical dimensions but different surface qualities at the joint contact interface are considered. The contact surfaces corresponding to assembled structures are finished by different methods (Table 2) and their roughness is measured. A high-resolution profile-meter (i.e. Surfscan 200) with a $12.5\mu m$ end-tip is employed to assess the roughness of the contact interfaces. The rectangular contact surfaces of each test structure are partitioned into grids of smaller areas and the roughness of each area is measured. The measured roughness values over the contact interface and a picture of the contact surfaces are shown in Figure 12.

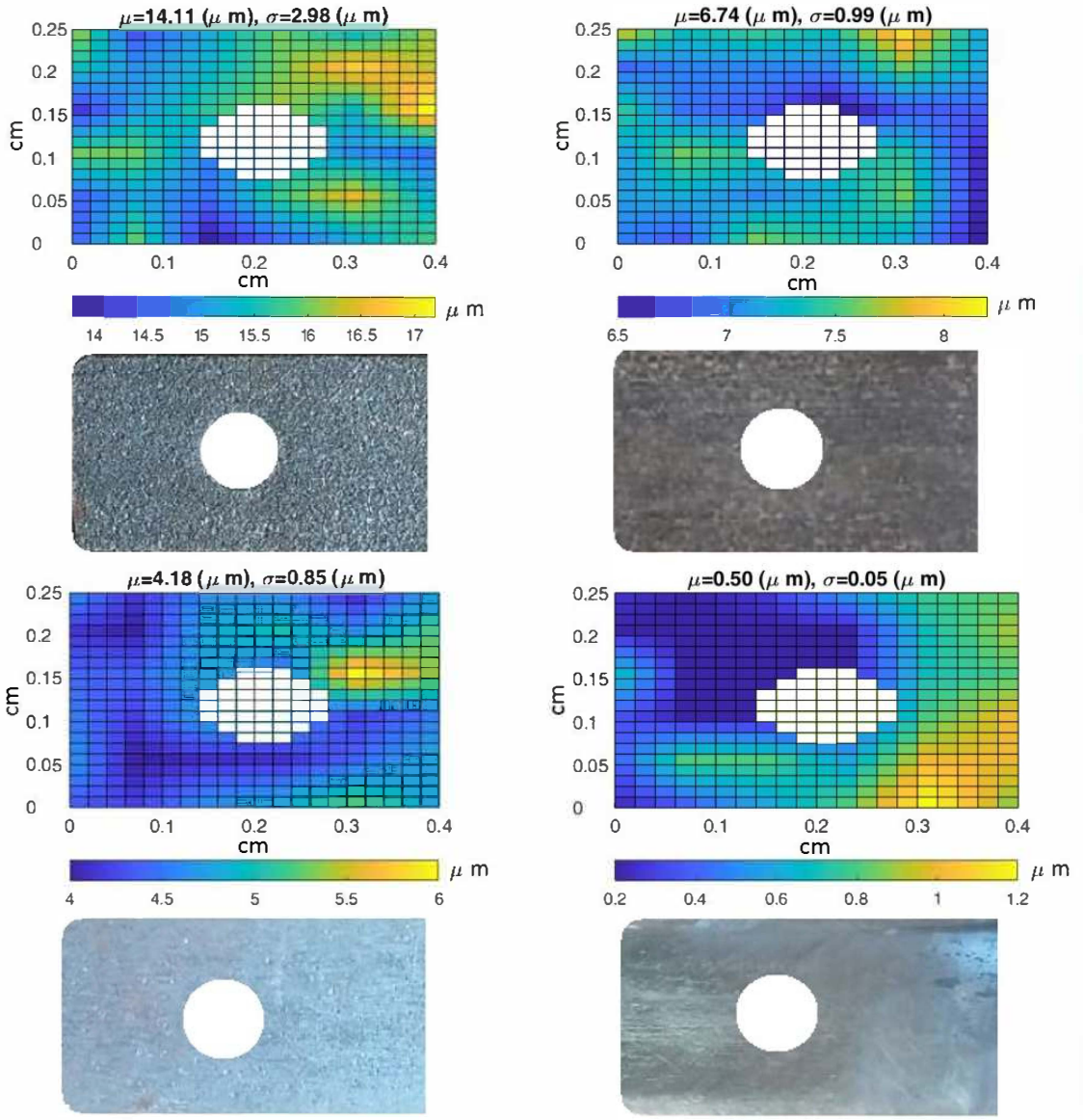

Figure 12. Measured roughness values over the contact interfaces

Table 2. methods used for preparing contact surfaces

	Surface finish method
Surface#1	Shot blasted
Surface#2	Original cold rolled stainless steel
Surface#3	Fine sandpaper polished
Surface#4	Extra-fine sandpaper polished

In Table 2, *Surface#1*, *Surface#2*, *Surface#3* and *Surface#4* refer to assembled structures having contact surfaces with mean roughness values (i.e. *SRM*) of 14.11, 6.74, 4.18 and 0.50 μm respectively (Figure 12). Two different bolt preloads, i.e. $P = 30$ N and $P = 50$ N, are considered for each assembled structure.

There are many methods to estimate the bolt preload, which have different accuracies. Examples that are frequently employed include a torque wrench, strain gages and measuring bolt elongation [45]. In this paper the bolt preload (or tension) is applied by tightening the nut with a torque wrench. The relationship between the bolt tension, F_{PT}, and the applied torque, T, is [46],

$$T = \kappa \, d_b \, F_{PT} \tag{43}$$

where κ is the nut factor (an average value of $\kappa = 0.2$ is used in this paper) and d_b is the diameter at the small end of the bolt ($d_b = 8$ mm).

Experimental modal testing is performed on the assembled structures to measure their dynamic properties, i.e. FRFs. Since measurement of FRFs is usually done with free-free boundary conditions, soft rubber bands are used to suspend the test structures to achieve this condition. To measure the bending natural frequencies of the assembled structures, a 8702B100M1 KISTLER piezoelectric accelerometer is attached to the structure using wax. An impact hammer including a KISTLER force transducer of type 9712B50 is used to excite the structure. Since the linear behaviour of the assembled structures is of interest, low level excitation forces (i.e. ~ 20 mN) are applied to the structures. The symmetry of the FRFs around resonant points (i.e. Figure 13) at this excitation force level assures that the structure behaves linearly for the preloads considered in this paper. It is worth mentioning that since the linear joint model proposed in this paper doesn't consider interfacial kinematics, it is very important to excite the structure such that separation of the contacting surfaces in the normal direction or micro/gross slip in the tangential direction does not happen. Force and acceleration type response signals are measured and transferred to a National Instrument data acquisition board type NI USB-4432. The signals are sampled at a sample rate of 1600 Hz and are then inputted into LabView signal processing software to calculate the frequency response functions (FRFs). The test structure is shown in Figure 13 and some measured FRFs are shown in Figure 14.

Figure 13 – Experimental test set-up: beam structures (a), accelerometer (b) and data acquisition and hammer (c)

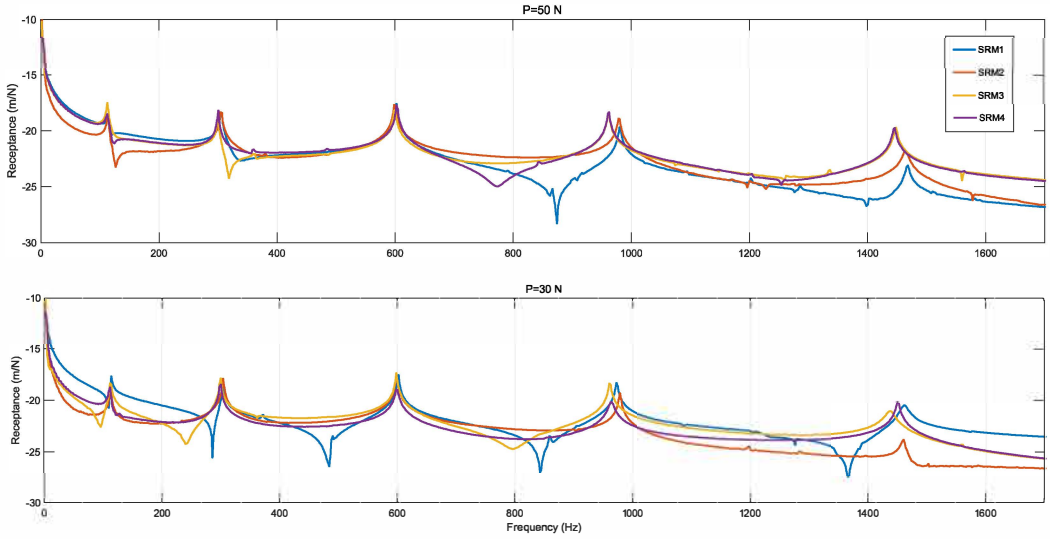

Figure 14. Measured FRFs for different contact surface qualities and different preloads

Since the method proposed in this paper is based on natural frequencies, the peak picking method is used to extract the natural frequencies by using the measured FRFs. The other reason that peak picking can be used is that the assembled

structures have well-separated modes, as shown in Figure 13. Therefore, around each resonance, the FRFs are dominated by the contribution of one vibration mode and the contributions of other vibration modes are negligible. This ensures that the measured FRFs can be treated as the FRF from an SDoF system and the mathematical model of the SDoF system can then be curve fitted onto measured FRFs to derive the modal parameters. Figure 15 shows the experimental natural frequencies for different contact surface roughness qualities and preloads.

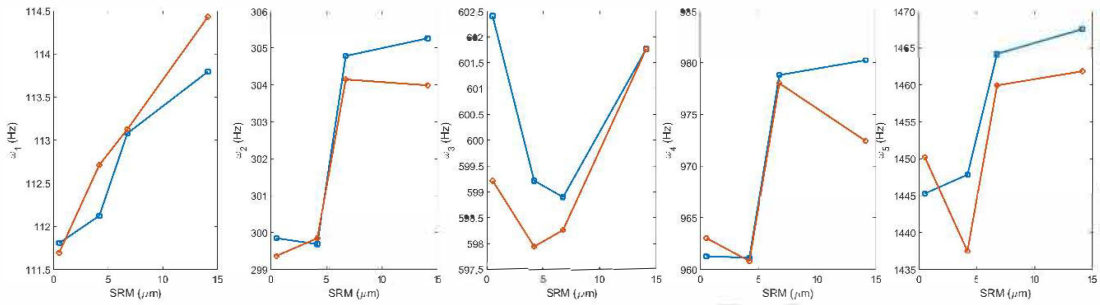

Figure 15. Natural frequencies at different contact surface roughness qualities and preloads, (o) P=30 N and (▫) P=50N.

Figure 15 shows that except for the first natural frequency, all other natural frequencies increase by increasing the bolt preload. Also, overall, by increasing the surface roughness mean value *SRM*, the first, second, fourth and fifth natural frequencies increase but the third natural frequency initially decreases and then increases. This indicates complexity in the physics of the contact interface. In other words, different parameters govern the behaviour of the contact interface.

To estimate the effects of preload and surface roughness quality on the damping in the contact interface, the quality (damping) factor Q is calculated for the third and fourth modes by using the half-power bandwidth method [47]. It is worth mentioning that for systems with light damping $Q \approx 2\zeta$, where ζ is the damping ratio. Changes in the quality factors for modes 3 and 4 are shown in Figure 16. Around the third and fourth natural frequencies, a good estimate of the FRFs are achievable by employing curve fitting, and hence only these two modes are used in quality factor extraction.

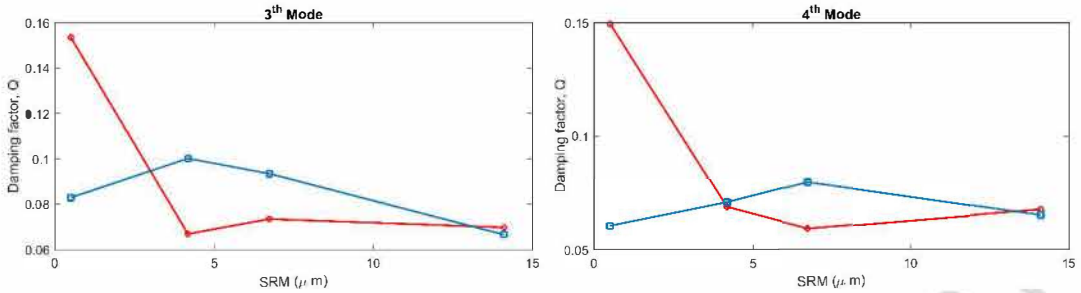

Figure 16. Damping factors at different contact surface roughness qualities and preloads, (o) P=30 N and (▫) P=50N.

Figure 16 indicates a complex behaviour for damping mechanism at the contact interface where both preload and surface roughness quality have great effects on the damping in the contact interface.

Next, identification of the joint model parameters is considered using the experimental results presented in Figure 15. Finite element models similar to those schematically shown in Figure 2 and mathematically described in Equation (37) for the numerical case study are constructed for each assembled structure using the beam and joint elements described in the previous sections. A reasonably fine mesh is used in the FE modelling of beam sections to keep the discretization error at a minimum level. Also, the material properties of the beam sections are obtained by comparing the experimental natural frequencies of one single beam with its FE correspondents. The material properties are considered as $E = 210$ GPa and $\rho = 7800$ kg/m^3. In the FE model, the mass effects of the bolt and nut are considered as a lumped mass element with mass and inertia of $m_b = 0.158$ g and $I_b = 0.003$ g.m^2 respectively. The sensitivity method described in Equations (30) to (32) is used to identify the joint parameters of different joint models by comparing experimental and FE natural frequencies. The joint parameters identified for different joint models are shown in Figure 17.

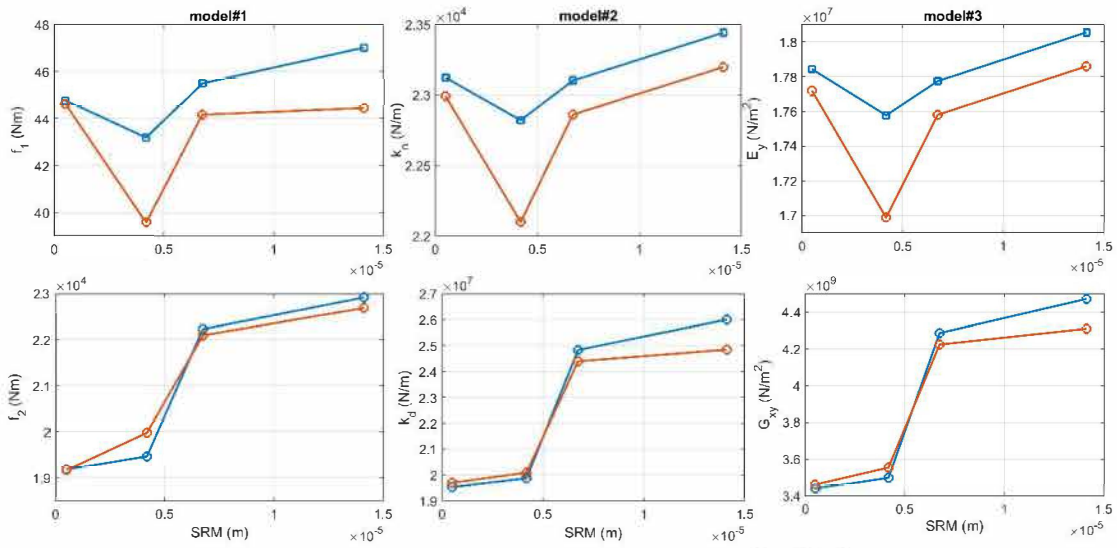

Figure 17. Identified joint model parameters for different contact surface roughness qualities and preloads, (o) P=30 N and (▫) P=50N.

Figure 17 shows that overall, the joint parameters defining normal stiffness of the contact interface, i.e. f_1, k_n and E_y, are affected more by changing the preload than the surface roughness quality. Moreover, the surface roughness quality affects the shearing stiffness of the contact interface the most. That is because there is greater change in the joint parameters defining the shearing stiffness of the contact interface, i.e. f_2, k_d and G_{xy}, when surface roughness mean value changes.

In Figure 18, the norms of the vector of differences between the experimental and identified natural frequencies for different models are shown.

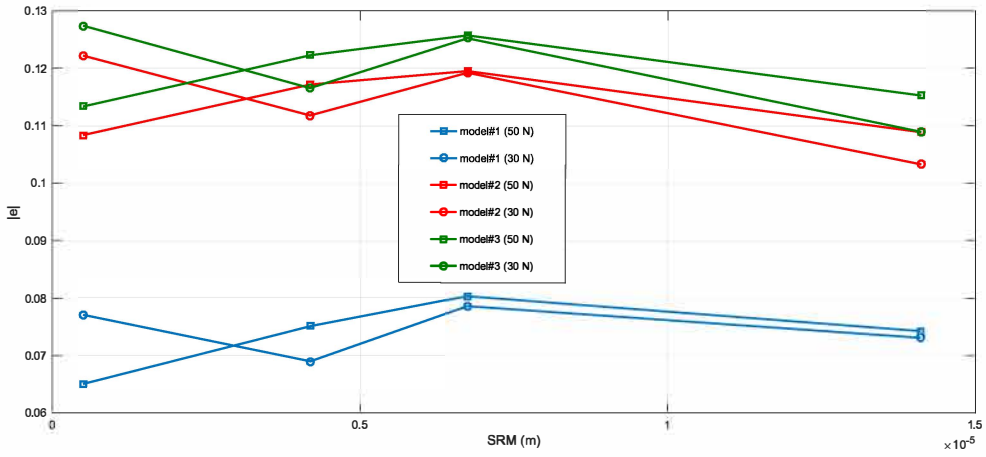

Figure 18. Norms of the error vector between identified and experimental natural frequencies

As Figure 18 shows, the beam-like generic joint model has the minimum norm of error. The errors of rectangular generic joint element proposed in this paper and the model proposed by Bograd et al. [14] are quite the same. All models can effectively identify the experimental results.

Finally, the mode shapes of the beam structure (Figure 11), which is modelled by the joint element proposed in this paper, are shown in Figure 19.

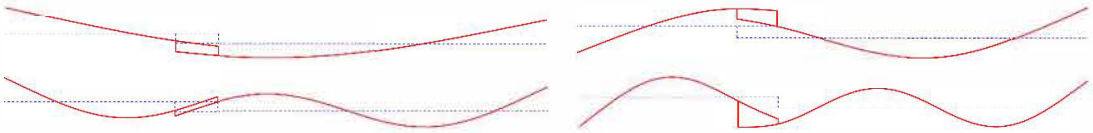

Figure 19. Mode shapes of the identified FE model for $P = 30$ N and $SRM = 14.11$ μm

The joint section in Figure 19 is modelled by using 16 joint elements, and Figure 19 indicates that the joint elements are subjected to both normal and shearing deformations in different modes.

8. Conclusions

This paper investigates on the capability of different joint models, including a new joint model introduced in this paper, to capture the effects of preload and surface roughness quality in dynamic modelling of assembled structures. A new joint model was proposed based on the stiffness matrix decomposition and the nature of the mechanisms involving in the contact interfaces. Both numerical and experimental results were used to investigate the effects of surface roughness quality and preload on identified joint model parameters and hence to evaluate the accuracy of the joint models.

In the numerical case study, the contact between two rough surfaces was modelled by using spring elements in three different directions. The joint models can capture the effect of the change in preload being represented by the stiffness of the spring elements. It was discussed that since one parameter, i.e. the preloads, governs the state of the contact interface in the numerical example, only one parameter dominates the dynamic behaviour of the joint models. Numerical simulation was also used to check the capability of the proposed damping model in predicting the energy dissipation at the contact interface.

In the experimental case study, four different assembled structures, similar in geometric properties but different in the joint contact interface, were considered. The contact surface of each beam structure was prepared by using a different surface finishing method. The natural frequencies of the test structures were measured under two different bolt preloads. Again, the joint models successfully captured the stiffness effect caused by the bolt pre-load and surface roughness quality. The identified results show that the parameter representing the normal stiffness of the contact interface in the joint models is more dominated by contact interface preload. Also, the surface roughness quality mostly controls the parameter representing the shear stiffness of the contact interfaces in the joint model parameters. The validity of the proposed joint models and the dynamic models identified for the assembled structure is restricted to the linear response of the structures.

Acknowledgment

This research is funded by the Engineering and Physical Sciences Research Council through Grant no. EP/P01271X/1.

References

[1] A. A. Ferri, "Friction damping and isolation systems," *Journal of Engineering for Gas Turbines and Power,* vol. 117, pp. 196-206, 1995.

[2] E. J. Berger, "Friction modeling for dynamic system simulation," *Appl. Mech. Rev.,* vol. 55, no. 6, pp. 535-577, 2002.

[3] R. A. Ibrahima and C. L. Pettit, "Uncertainties and dynamic problems of bolted joints and other fasteners," *Journal of Sound and Vibration,* vol. 279, no. 3-5, pp. 857-936, 2005.

[4] M. R. Brake, P. Reuss, D. J. Segalman and L. Gaul, "Variability and Repeatability of Jointed Structures with Frictional Interfaces," *Dynamics of Coupled Structures,* vol. 1, pp. 245-252, 2014.

[5] M. Hanss, S. Oexl and L. Gaul, "Identification of a bolted-joint model with fuzzy parameters loaded normal to the contact interface," *Mechanics Research Communications,* vol. 29, p. 177–187, 2002.

[6] R. E. Goodman, R. L. Taylor and T. L. Brekke, "A model for the mechanics of jointed rock," *Journal of the Soil Mechanics and Foundations Division, American Society of Civil Engineers ASCE,* vol. 94, p. 637–660, 1968.

[7] J. Geisler and K. Willner, "Modeling of jointed structures using zero thickness interface elements," *Proceedings in Applied Mathematics & Mechanics,* vol. 7, no. 1, p. 4050009–4050010, 2007.

[8] D. Süß, J. Geisler and K. Willner, "Numerical and experimental investigations of dynamic contact phenomena in jointed structures," *Proceedings in Applied Mathematics & Mechanics,* vol. 10, p. 263 – 264, 2010.

[9] M. H. Mayer and L. Gaul, "Segment-to-segment contact elements for modelling joint interfaces in finite element analysis," *Mechanical Systems and Signal Processing,* vol. 21, pp. 724-734, 2007.

[10] C. Desai, M. Zaman, J. Lightner and H. Siriwardane, "Thin-layer element for interfaces and joints," *International Journal for Numerical and Analytical Methods in Geomechanics,* vol. 8, p. 19–43, 1984.

[11] K. Sharma and C. Desai, "Analysis and implementation of thin-layer element for interfaces and joints," *Journal of Engineering Mechanics 1,* vol. 118, p. 2442–2462, 1992.

[12] H. Ahmadiana, J. E. Mottershead, S. James, M. I. Friswell and C. A. Reece, "Modelling and updating of large surface-to-surface joints in the AWE-MACE structure," *Mechanical Systems and Signal Processing,* vol. 20, p. 868–880, 2006.

[13] S. Bograd, A. Schmidt and L. Gaul, "Joint damping prediction by thin layer elements," in *International Modal Analysis Conference IMAC XXVI*, Orlando, 2008.

[14] S. Bograd, P. Reuss, A. Schmidt, L. Gaul and M. Mayer, "Modeling the dynamics of mechanical joints," *Mechanical Systems and Signal Processing,* vol. 25, pp. 2801-826, 2011.

[15] R. D. Mindlin, "Compliance of elastic bodies in contact," *Journal of Applied Mechanics,* vol. 71, pp. 259-268, 1949.

[16] J. A. Greenwood and J. B. P. Williamson, "Contact of nominally flat surfaces," *Proceedings of The Royal Society A,* vol. 295, pp. 300-319, 1966.

[17] K. Johnson, Contact Mechanics, Cambridge: Cambridge University Press, 1987.

[18] J. Krolikowski and J. Szczepek, "Assessment of tangential and normal stiffness of contact between rough surfaces using ultrasonic method," *Wear,* vol. 160, no. 2, pp. 253-258, 1993.

[19] R. A. Onions and J. F. Archard, "The contact of surfaces having a random structure," *Journal of Applied Physics,* vol. 6, pp. 289-304, 1973.

[20] H. A. Sherif and S. S. Kosa, "Relationship between normal and tangential contact stiffness of nominally flat surfaces," *Wear,* vol. 151, pp. 49-62, 1991.

[21] M. Gonzalez-Valadez, A. Baltazar and R. S. Dwyer-Joyce, "Study of interfacial stiffness ratio of a rough surface in contact using a spring model," *Wear,* vol. 268, no. 3-4, pp. 373-379, 2010.

[22] M. L. Raffa, F. Lebon and G. Vairo, "Normal and tangential stiffnesses of rough surfaces in contact via an," *International Journal of Solids and Structures,* vol. 87, pp. 245-253, 2016.

[23] D. Goerke and K. Willner, "Investigations of the influence of geometrical irregularities and roughness on the normal contact stiffness of joints," *Proceedings in Applied Mathematics & Mechanics,* vol. 8, p. 10275 – 10276, 2008.

[24] D. J. Segalman, T. L. Paez, D. O. Smallwood, A. H. Sumali and A. Urbina, "Status and Integrated Road-Map for Joints Modeling Research," Report No. SAND2003-0897, Sandia National Laboratories, 2003.

[25] X. Ma, L. Bergman and A. Vakakis, "Identification of bolted joints through laser vibrometry," *Journal of Sound and Vibration,* vol. 246, p. 441–460, 2001.

[26] H. Jalali, H. Ahmadian and F. Pourahmadian, "Identification of micro-vibro-impacts at boundary condition of a nonlinear beam," *Mechanical Systems and Signal Processing,* vol. 25, no. 3, pp. 1073-1085, 2011.

[27] L. Gaul and J. lenz, "Nonlinear Dynamics of Structures Assembled by Bolted Joints," *Acta Mechanica,* vol. 125, no. 4, pp. 169-181, 1997.

[28] H. Ahmadian, H. Jalali and F. Pourahmadian, "Nonlinear model identification of a frictional contact support," *Mechanical Systems and Signal Processing,* vol. 24, no. 8, pp. 2844-2854, 2010.

[29] I. R. Grosse and L. D. Mitchell, "Nonlinear axial stiffness characteristics of axisymmetric bolted joints," *American Society of Mechanical Engineers, Journal of Mechanical Design,* vol. 112, pp. 442-449, 1990.

[30] F. Pourahmadian, H. Ahmadian and H. Jalali, "Modeling and identification of frictional forces at a contact interface experiencing micro-vibro-impacts," *Journal of Sound and Vibration,* vol. 331, no. 12, pp. 2874-2886, 2012.

[31] H. Ahmadian, M. Ebrahimi, J. E. Mottershead and M. I. Friswell, "Identification of bolted-joint interface models," in *International Conference on Noise and Vibration Engineering ISMA*, Leuven, 2002.

[32] H. Ahmadian, H. Jalali, J. E. Mottershead and M. I. Friswell, "Dynamic modelling of spot welds using thin layer interface theory," in *10th International Congress on Sound and Vibration*, Stockholm, 2003.

[33] H. Jalali, A. Hedayati and H. Ahmadian, "Modelling mechanical interfaces experiencing micro-slip/slap," *Inverse Problems in Science and Engineering,* vol. 19, no. 6, pp. 751-764 , 2011.

[34] M. Iranzad and H. Ahmadian, "Identification of nonlinear bolted lap joint models," *Computers and Structures,* vol. 96–97, pp. 1-8, 2012.

[35] D. Süß, M. Jerschl and K. Willner, "Calculating the Dynamic Response of Jointed Structures in the Frequency Domain Using Contact Interface Elements," in *The Mechanics of Jointed Structures*, Cham, Springer, 2018, pp. 491-510.

[36] H. Ahmadian and H. Jalali, "Generic element formulation for modelling bolted lap joints," *Mechanical Systems and Signal Processing,* vol. 21, pp. 2318-2334, 2007.

[37] G. H. Golub and C. F. Van Loan, Matrix Computations, Baltimore: JHU Press, 2012.

[38] G. W. Stewart, Introduction to Matrix Computations, London: Academic Press, 1973.

[39] S. W. Doebling, L. D. Peterson and K. F. Alvin, "Experimental determination of local structural stiffness by disassembly of measured flexibility matrices," *Journal of Vibration and Acoustics,* vol. 120, pp. 949-957, 1998.

[40] G. M. L. Gladwell and H. Ahmadian, "Generic element matrices suitable for finite element model updating," *Mechanical Systems and Signal Processing,* vol. 9, no. 6, pp. 601-614, 1995.

[41] O. C. Zienkiewicz and R. L. Taylor, The finite element method, Stonham: Butterworth-Heinemann, 2000.

[42] S. Medina, D. Nowell and D. Dini, "Analytical and Numerical Models for Tangential Stiffness of Rough Elastic Contacts," *Tribology Letters,* vol. 49, no. 1, pp. 103-115, 2013.

[43] N. Yoshioka and C. H. Scholz, "Elastic properties of contacting surfaces under normal and shear loads: 1. Theory," *Journal of Geophysical Reseach: Solid Earth,* vol. 94, no. B12, p. 17681–17690, 1989.

[44] M. I. Friswell and J. E. Mottershead, Finite Element Model Updating in Structural Dynamics, Netherlands: Kluwer Academic Publishers, 1995.

[45] E. Oberg, J. F, H. Horton and H. Ryffel, Machinary Handbook, New York: Industrial Press Inc., 2004.

[46] J. E. Shigley, C. R. Mischke and T. H. Brown, Standard handbook of machine design, Third edition, New York: McGRAW-HILL, 2004.

[47] W. T. Thomson, Theory of vibration with applications (4th ed), New Jersey: Prentice Hall, 1993.

A new joint model representing surface roughness and preload effects is introduced.

Joint element stiffness model is obtained using decomposition of stiffness matrix.

The accuracy of the joint model is assessed using numerical and experimental data.

Experimental data reveal a complex mechanism for energy dissipation in the joint.